THE EFFECT OF ARC-BASED DIRECT METAL ENERGY DEPOSITION ON PBF MARAGING STEEL

Bishal Silwal*, Christopher Gerdmann*, Stephen Migues*, Kamram Kardel**, Shaowen Xu*
Andrew Durrence***

*Department of Mechanical Engineering, Georgia Southern University, Statesboro, GA, 30460
**Department of Manufacturing Engineering, Georgia Southern University, Statesboro, GA, 30460
*** Gulfstream Aerospace, Savannah, GA

Abstract

With the growing demand of metal based additive manufacturing it is inevitable that the additively manufactured parts will be used in consolidation with different manufacturing process. Arc based additive manufacturing is a process used to produce three-dimensional structure using welding arc as a power source. Powder Bed Fusion (PBF) is an additive manufacturing process using laser power to generate a three dimensional structure. In this paper, the effect of direct energy deposition on the PBF has been investigated. The microstructure changes and the melting region are characterized. A computational fluid dynamics model is used to predict the melt region and temperature in PBF.

Keywords: *Additive manufacturing, welding arc, GTAW, ABAM, Maraging Steel, PBF*

Introduction

The additive manufacturing (a.k.a 3d printing) industry generated over $5 billion in 2015 and is expected to grow over five times by year 2021 [4]. According to ASTM, there are seven categories of additive manufacturing: photopolymerization, material jetting, binder jetting, material extrusion, powder bed fusion, sheet lamination and direct enegy deposition. Based upon the power source and feed material, it can be further classified into many individual processes (Figure 1).

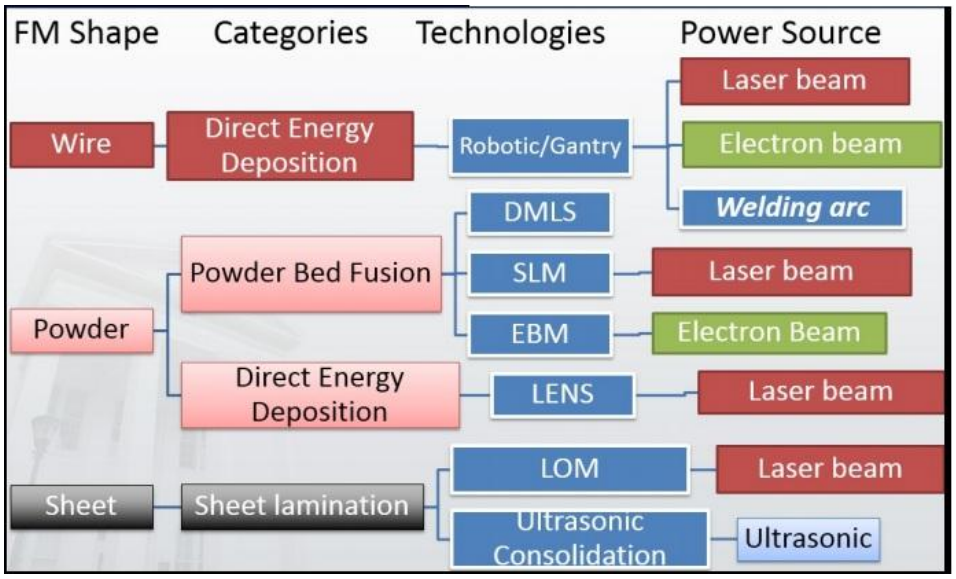

Figure 1: Additive manufacturing technology based upon the power source and feed material shape [12]

Powder bed fusion (PBF) is one of the many commercially available additive manufacturing (a.k.a 3-d printing) technologies to fabricate net shape parts. In this process, a thin layer of powder on powder-bed is slectively melted by laser, building a volume on a layer-by-layer basis. The major advantage of using PBF is that a complex geometry can be acheived which may yield longer time by using other conventional manufacturing technologies.

Arc based additive manufacturing (ABAM) is a process in which a welding arc used as a power source to melt the substrate and filler-wire. The tool path can be generated via an industrial robot, numerical controlled gantry system or a Rep-Rap system. The deposition rate of 10-20 lbs/hr can be achieved in this process, which is promising in large structure fabrication. Two of the main challenges restricts its' use in AM industry are lower resolution of layer height (compared to PBF) and lack of technical resource (mainly path planning) for complex geometry.

Maraging steels offer combination of excellent material properties such as tensile strength, fracture toughness, dimensional stability and good weldability. These steels are extensively used in aerospace and tooling industries. There are four principal grades of wrought 18% nickel maraging steels; designated as Grades 200, 250, 300 and 350 based upon their tensile strength value in English units. The primary microstructure of the maraging steel is a martensite matrix with precipitation of intermetallic compounds such as Ni_3Ti, Fe_2Mo etc. It has also reported that due to formation of retained austenite during aging, the mechanical properties such as tensile and toughness improves [5]. Many researchers have investigated the mechanical properties of the DMLS produced maraging steel [1, 3]. The precipitation hardening behavior has also been studied in the past [2]. Based upon the observation from [2], the as-fabricated PBF maraging steel has martensite matrix with small regions of retained austenite. In order to improve the structural properties, further processing such as shot peening, welding and heat treatment etc of PBF fabricated part are unavoidable in manufacturing. In this paper, the effect of welding arc deposited maraging wire on PBF fabricated part is studied. A cold-wire Gas Tungsten Arc Welding (GTAW) has been used as a heat source. The surface texture, macro and microstructure and hardness of PBF fabricated maraging steel have been carried out.

The numerical modeling in PBF is less computationally efficient due to the nature of the complexity and fineness involved. Lee et al. [6] has used the mesoscale model to predict the fluid flow, temperature and solidification in nickel based alloy. The powder packing model was developed using the discrete element method (DEM) [6]. More detail literature review on the aspect of numerical modeling has been found on [7, 8, and 9]. In this paper, a computationally efficient model is developed using a uniform particle bed, recoil pressure, evaporative pressure, Fresnel reflection and Gaussian distribution of laser heat source.

Experimental

The experiment was performed in EOSINT M 280. The material composition of maraging part (Grade 300) is presented in Table 1. The EOS parameters are presented in Table 2. The built volume was 4.00×1.75×0.30 inches. The surface texture was measured by using Keyence digital profilometer. After built, one part was cut off (0.50×1.75×0.30) from the base metal (substrate) using a horizontal band saw. The layer deposition was performed using cold-wire GTA on the part with the maraging wire identical in composition to maraging powder. The parameters for GTA process were: 3 mm/sec travel speed, 150 A welding current and 26 mm/sec wire feed speed. An argon gas with flow rate of 15 liter per minute was used as a shielding gas.

Table 1: The chemical composition of the Grade 300 maraging steel

Grade	Al	C	Co	Fe	Mn	Mo	Ni	P	S	Si	Ti
Maraging	0.05-0.15	0.003	8.5-9.5	Bal	0.1	4.60 5.20	17.0-19.0	0.01	0.01	0.1	0.6-0.8

Table 2: The parameters in DMLS

Parameters	Values
Powder size	~30 micron
Focus Diameter	100-500 Ωm
Laser power	200 W
Scan speed	NA
GTA travel speed	3 mm/sec
GTA Power Input	2700 W
GTA Wire feed speed	26 mm/sec

Results and Discussion

The as-built unpolished surface profile measurement is presented in Figure 2. The surface roughness has the maximum value of 25.73 µm and minimum value of 20.38 µm. The micrograph is presented in the right side of the Figure 2, while the contour variation of surface topography is presented in the left side of the Figure 2. The arrow indicates the built direction. The darker regions

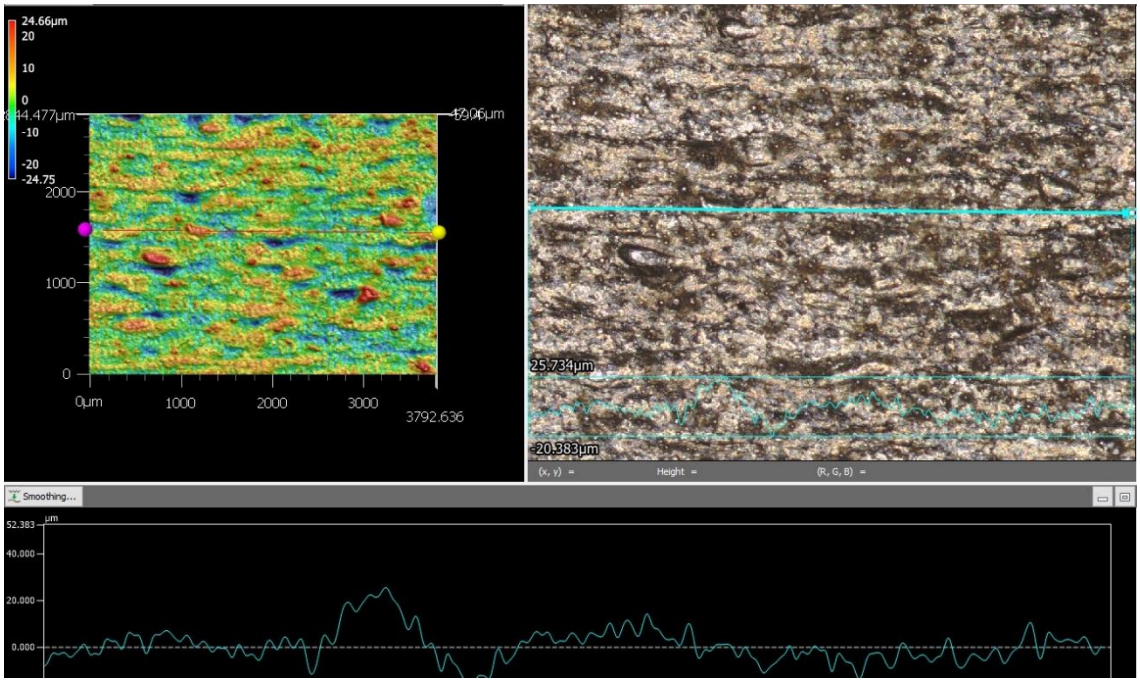

Figure 2: The surface topography measurement of PBF maraging steel

as seen on the micrograph have higher value while the brighter regions have lower value. It may be due to re-melting of the layer, which let the fluid to flow outward. The average layer thickness is ~ 100 micron. The adsorbed powders are also visible on the micrograph (Figure 3)Figure 3: The built direction with multiple layers on left and higher magnification on the right depicting the non-uniformity of the individual layer. It is also clear from the figure that the layers are non-uniform. The primary reason is due to powder size distribution and powder arrangement which affect the laser power absorption. In addition, melting of powder, remelting of the solidified layer and fluid flow of the molten metal due to Maragoni effect and capillary effect play important role in the final shape of the solidified layer.

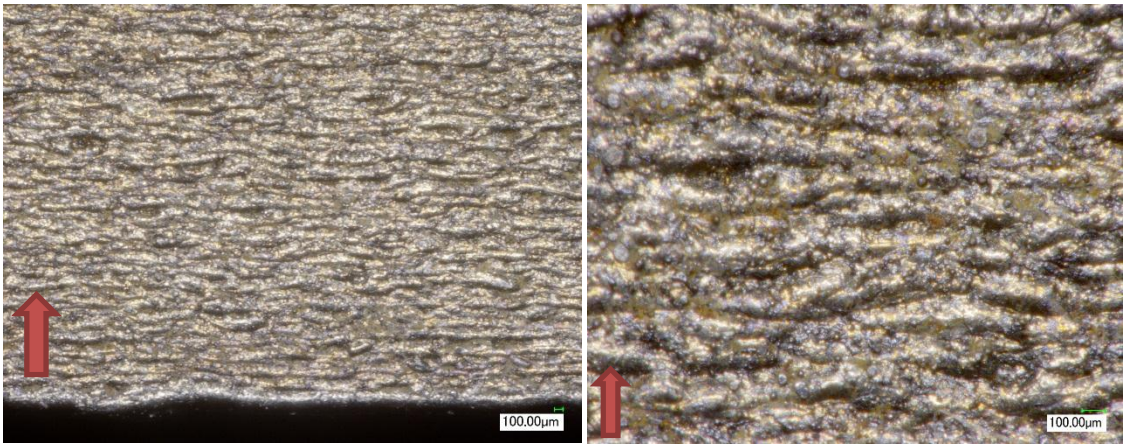

Figure 3: The built direction with multiple layers on left and higher magnification on the right depicting the non-uniformity of the individual layer and adsorbed powder

The Rockwell hardness is presented in Figure 3. The hardness value is within the range of 31 to 37 HRC in the PBF maraging steel. The Gas Tungsten Arc (GTA) deposited maraging steel has the hardness value ranges from 16 to 23 HRC. The heat affected region of maraging steel has hardness of 28-29 HRC. The GTA heat has definitely decrease the hardness of the PBF maraging steel from 34 average HRC to 28 HRC.

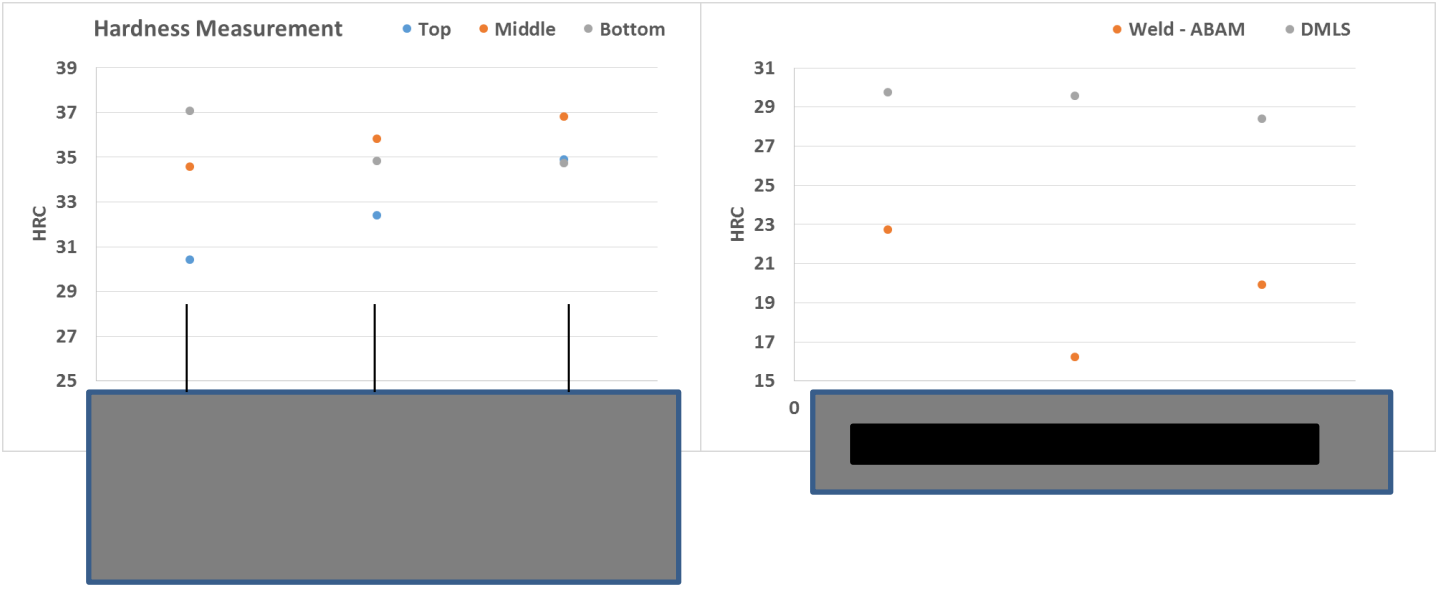

Figure 4: Rockwell hardness measurement: Powder Bed Fusion (PBF) maraging steel on left and GTA direct deposition on the right (the darker area represents the layer deposited by GTA)

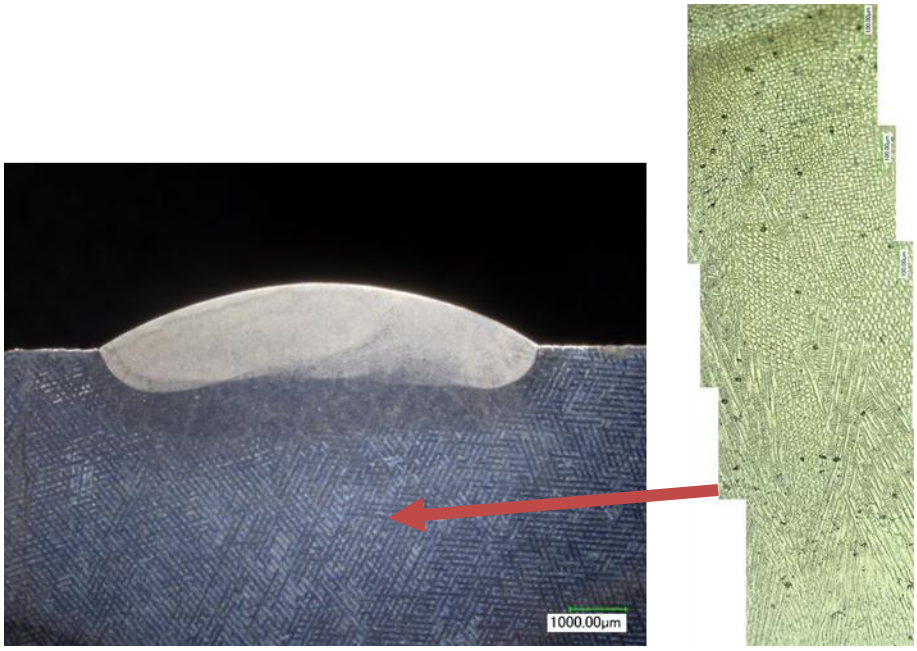

Figure 5: The micrograph of the GTA deposited maraging steel

The GTA deposited surface is presented in Figure 5. The layer is nearly 800 µm, which is 8-9 times bigger than the average layer of PBF. A metallurgical bonding has been observed. The solidification morphology entails an epitaxial growth with planar-columnar in the joint, then columnar and equiaxed dendrite towards the outward region as depicted in Figure 5. The solidification morphology of the PBF maraging steel is not conclusive, however some columnar grain is visible in the micrograph presented in the Figure 6. The energy-dispersive X-ray spectroscopy (EDX) analysis was performed on the PBF layers. The results, mainly chemical composition is presented in Table 3. There is no significant difference, however small difference of nickel content was observed. The area 'A' represents some fine grains (not visible in Figure 6) while 'B' represents columnar grains.

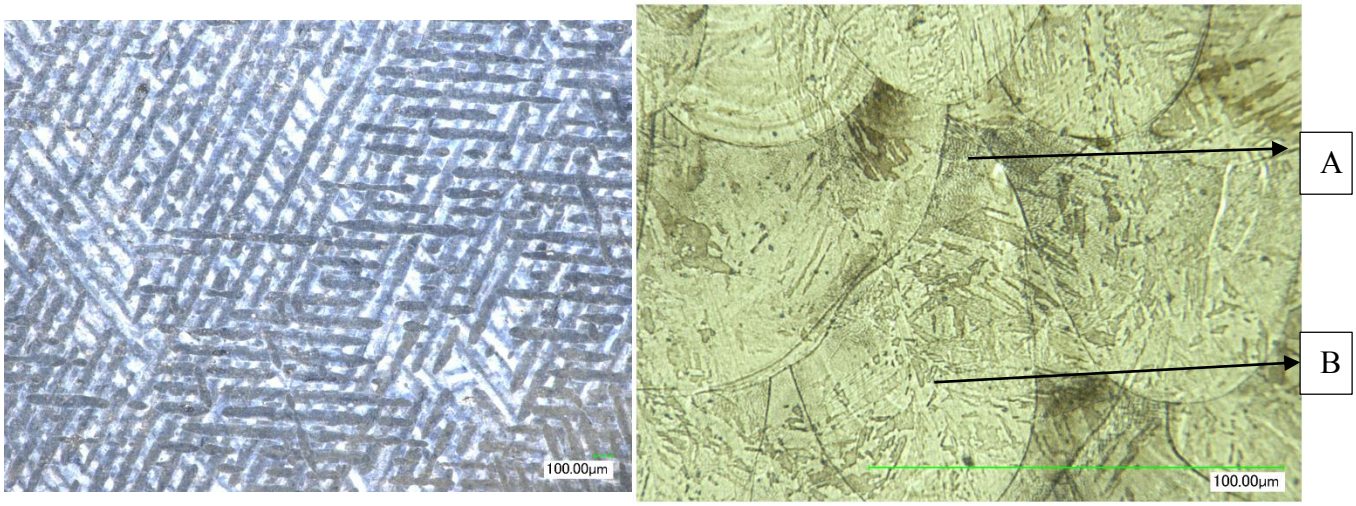

Figure 6: The micrograph of PBF maraging steel, wire EDM cut, polished and etched (left), transverse direction on the right at higher magnification

Table 3: EDX analysis of the PBF layers

Map Sum Spectrum	A (Wt%)	B (Wt%)
O	1.16	1.56
F	1.18	NA
Al	0.37	0.22
Si	0.28	0.28
Ti	0.62	0.58
Fe	66.81	67.44
Co	7.08	7.28
Ni	15.34	14.65
Mo	3.97	3.91
S	NA	0.05

Mathematical Model

The mathematical model for GTA deposition has been presented in [11]. In this paper, the phenomenon in PBF with high heating of laser power has been considered. The laser sintering involves laser-powder interaction, phase change, heat and mass transfer and fluid flow. A computation domain of 1000 x 140 x 120 micron is considered. A 30 micron layer of uniform diameter powder particles is considered. The laser beam profile is assumed as a Gaussian type axisymmetric distribution. The distribution equation of laser energy is described as

$$q(r) = Qe^{(-\frac{r}{r_b})^2}$$

where, q denotes heat density function, Q is the total power of the laser beam, r is the coordinate in radial direction and r_b is the laser beam radius at focus plane. The melting temperature and melt pool velocity are calculated using the conservation of momentum, conservation of energy and material continuity equations. The convection, conduction, radiation and evaporative boundary conditions are applied. The surface tension force is also applied as a boundary condition. The VOF method is used to track the free surface. The numerical model consist of two region of 30 mm x 4 mm x 3 mm and constant diameter powder region with same stack size. The recoil pressure is calculated using,

$$P_r = Ae^{\{B\left(1-\frac{T_v}{T}\right)\}}$$

Where, P_r is recoil pressure, T_v is evaporation temperature, T is the surface temperature, A and B are material dependent coefficients taken as 3500 and 5.

The absorption rate (Fresnel reflection) is calculated from

$$a = 1 - \frac{1}{2}\left(\frac{1+(1-\varepsilon cos\phi)^2}{1+(1+\varepsilon cos\phi)^2} + \frac{\varepsilon^2 - 2\varepsilon cos\phi + 2cos^2\phi}{\varepsilon^2 + 2\varepsilon cos\phi + 2cos^2\phi}\right)$$

where, ε is the coefficient dependent upon laser type, φ is the angle between incident and surface normal. The heat flux is further calculated using, $q_n = q_{n-1} * \alpha_n$. The loop is performed until the heat flux becomes small.

,

The saturated vapor pressure is given by,

$$P_s = Pe^{\{\lambda\left(\frac{1}{T_b} - \frac{1}{T}\right)\}}$$

Where, P_s is the saturated vapor pressure, P is the atmospheric pressure, T_b is the boiling temperature, T is the surface temperature, and λ is the evaporation energy per atom. The equation below is used to calculate the mass transfer due to evaporation and calculated based on the kinetic theory

$$M_{net} = R_{accom}\sqrt{\frac{M}{2\pi RT}}(P_s - P_v)$$

Boundary Condition:

$$K\frac{\partial T}{\partial \vec{n}} + h(T_s - T) + Q_{vap} + \sigma\varepsilon(T_s^4 - T^4) = q(r)$$

$$\vec{F} = \vec{n}\nabla(\nabla\gamma) - \nabla_s\gamma$$

The first boundary equation is for the energy equation, where *K* is the thermal conductivity and assume to be constant, n is the normal vector, T_s is the surface temperature, Q_{vap} is heat loss due to vaporization, σ is the Boltzmann Constant, ε is the emissivity. The second boundary equation is for momentum equation in which the first term represents the surface tension force and the second term is due to surface tension gradient. The material properties is provided in Table 3.

Table 4: The material properties used in the numerical simulation

Parameters	Values
Density (kg/m^3)	7200
Viscosity	0.0075
Specific Heat (J/kg-K)	700
Latent Heat of Fusion (J/kg)	2.77 E05
Thermal conductivity (W/m-K)	30
Surface Tension (kg/s^2)	1.882
Liquidus Temperature (°C)	1600
Solidus Temperature (°C)	1500
Saturation Temperature (°K)	2300

Melt pool evolution:

The temperature profile is presented in Figure 7. The flow is more dependent upon the Maragoni convection and vapor pressure due to initial evaporation temperature assumption of ~ 2300 K for maraging steel. An additional melt region may have been achieved due to Fresnel reflection.

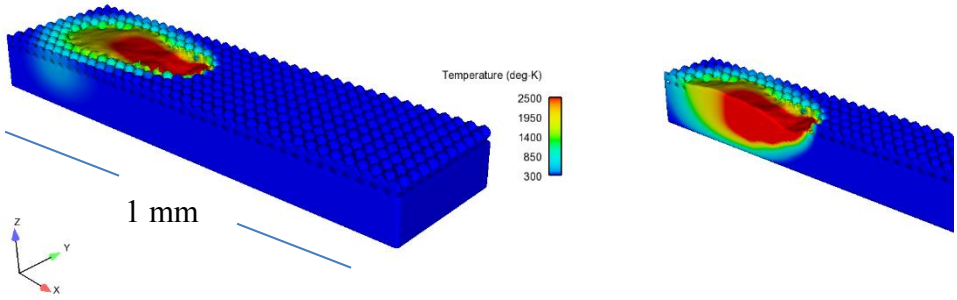

Figure 7: Temperature profile on the left and melt pool depth on the right

Conclusion

One layer of maraging steel has been deposited on the PBF maraging steel by arc based additive manufacturing (ABAM). The microstructure of the layer is martensitic with some retained austenite. The epitaxial growth follows a planar, columnar and equiaxed grain size. The Rockwell hardness value has been reduced due to the heat of ABAM process, thus softening and removing the laser (fish-scale) tracks on the PBF maraging steel. A high fidelity numerical model has been developed to predict the temperature and the melt pool shape for the PBF process. Future work will be focused on microstructural modeling and energy-dispersive X-ray spectroscopy analysis to differentiate the arc weld against the PBF maraging steel.

Acknowledgement

The authors would like to thank Dr. Rafael Quirino and Ms. Khristal Monroe from Chemistry Department at Georgia Southern for providing assistance in SEM use.

References

1. Kempen, K., Yasa, E., Thijs, L., Kruth, J. P., & Van Humbeeck, J. (2011). Microstructure and mechanical properties of Selective Laser Melted 18Ni-300 steel. *Physics Procedia*, *12*, 255-263.

2. Jägle, E. A., Choi, P. P., Van Humbeeck, J., & Raabe, D. (2014). Precipitation and austenite reversion behavior of a maraging steel produced by selective laser melting. *Journal of Materials Research*, *29*(17), 2072-2079.

3. Tan, C., Zhou, K., Tong, X., Huang, Y., Li, J., Ma, W., & Kuang, T. (2016). Microstructure and Mechanical Properties of 18Ni-300 Maraging Steel Fabricated by Selective Laser Melting.

4. Wohlers, T., 2016, Wohlers Report 2016: Additive Manufacturing and 3D Printing State of the Industry: Annual Worldwide Progress Report.

5. Abreu, H. F. G., Tavares, S. S. M., Silva, J. J. M., Menezes, J. W. A., & Bruno, A. D. (2004). The influence of an intermediate austenitization heat treatment in the texture of cold-rolled and aged 18% Ni maraging steel. Materials characterization, 52(3), 203-207.

6. Lee, Y. S., & Zhang, W. (2015). Mesoscopic simulation of heat transfer and fluid flow in laser powder bed additive manufacturing. In *International Solid Free Form Fabrication Symposium, Austin* (pp. 1154-1165)

7. Khairallah, S. A., Anderson, A. T., Rubenchik, A., & King, W. E. (2016). Laser powder-bed fusion additive manufacturing: Physics of complex melt flow and formation mechanisms of pores, spatter, and denudation zones. *Acta Materialia*, *108*, 36-45.

8. Babis Schoinochoritis, Dimitrios Chantzis, and Konstantinos Salonitis, "Simulation of metallic powder bed additive manufacturing processes with the finite element metho: A critical review," Institution of Mechanical Engineers, pp. 1-22, 2014.

9. W. E. King et al., "Laser powder bed fusion additive manufacturing of metals," Applied Physics Review 2, vol. 2, p. 041304, 2015

10. Cho, J. H., & Na, S. J. (2006). Implementation of real-time multiple reflection and Fresnel absorption of laser beam in keyhole. *Journal of Physics D: Applied Physics*, *39*(24), 5372.

11. Silwal, B., & Santangelo, M. (2017). Effect of vibration and hot-wire Gas Tungsten Arc (GTA) on the geometric shape. Journal of Materials Processing Technology, https://doi.org/10.1016/j.jmatprotec.2017.08.010.

12. Santangelo, M., Silwal, B., & Purdy, A. vibration assisted robotic hot-wire gas tungsten arc welding (GTAW) for additive manufacturing of large metallic parts, Solid FreeForm Symposium, Austin, 2016